Inorganic Chemistry

Article

pubs.acs.org/IC

Influence of an Inner-Sphere K^+ Ion on the Magnetic Behavior of N_2^{3-} Radical-Bridged Dilanthanide Complexes Isolated Using an External Magnetic Field

Katie R. Meihaus,[†,§] Jordan F. Corbey,[‡,§] Ming Fang,[‡] Joseph W. Ziller,[‡] Jeffrey R. Long,*[,†] and William J. Evans*[,‡]

[†]Department of Chemistry, University of California, Berkeley, California 94720-1460, United States

[‡]Department of Chemistry, University of California, Irvine, California 92697-2025, United States

Supporting Information

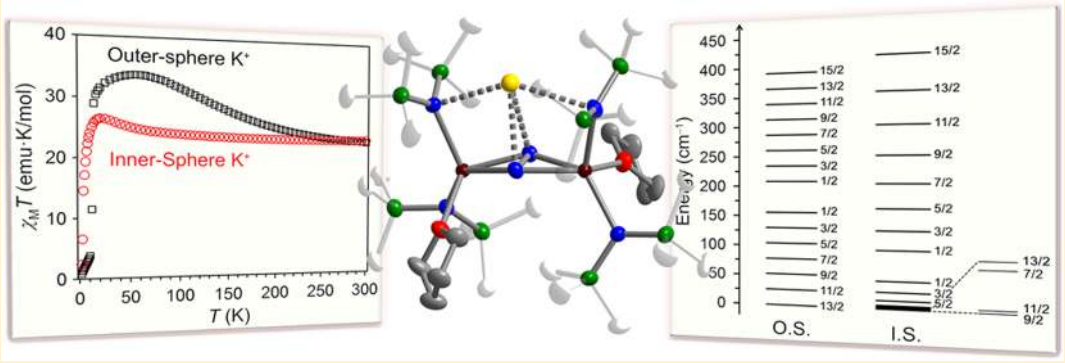

ABSTRACT: The synthesis and full magnetic characterization of a new series of N_2^{3-} radical-bridged lanthanide complexes $[\{(R_2N)_2(THF)Ln\}_2(\mu_3\text{-}\eta^2\text{:}\eta^2\text{:}\eta^2\text{-}N_2)K]$ [**1-Ln**; Ln = Gd, Tb, Dy; $NR_2 = N(SiMe_3)_2$] are described for comprehensive comparison with the previously reported series $[K(18\text{-crown-}6)(THF)_2]\{[(R_2N)_2(THF)Ln]_2(\mu\text{-}\eta^2\text{:}\eta^2\text{-}N_2)\}$ (**2-Ln**; Ln = Gd, Tb, Dy). Structural characterization of **1-Ln** crystals grown with the aid of a $Nd_2Fe_{13}B$ magnet reveals inner-sphere coordination of the K^+ counterion within 2.9 Å of the N_2^{3-} bridge, leading to bending of the planar Ln−(N_2^{3-})−Ln unit present in **2-Ln**. Direct current (dc) magnetic susceptibility measurements performed on **1-Gd** reveal antiferromagnetic coupling between the Gd^{III} centers and the N_2^{3-} radical bridge, with a strength matching that obtained previously for **2-Gd** at $J \sim -27$ cm^{-1}. Unexpectedly, however, a competing antiferromagnetic Gd^{III}−Gd^{III} exchange interaction with $J \sim -2$ cm^{-1} also becomes prominent, dramatically changing the magnetic behavior at low temperatures. Alternating current (ac) magnetic susceptibility characterization of **1-Tb** and **1-Dy** demonstrates these complexes to be single-molecule magnets under zero applied dc field, albeit with relaxation barriers (U_{eff} = 41.13(4) and 14.95(8) cm^{-1}, respectively) and blocking temperatures significantly reduced compared to **2-Tb** and **2-Dy**. These differences are also likely to be a result of the competing antiferromagnetic Ln^{III}−Ln^{III} exchange interactions of the type quantified in **1-Gd**.

INTRODUCTION

Unraveling the relationship between structure and magnetic properties is a fundamental goal in the study of lanthanide molecular magnetism. In mononuclear lanthanide species, the combination of inherently large magnetic anisotropy with the appropriate ligand field symmetry has been used to rationalize slow magnetic relaxation in many different coordination environments.[1] Even for multinuclear complexes, single-ion anisotropy and symmetry often trump exchange interactions as the most relevant criteria for promoting slow relaxation,[2] and this is due to the fact that the contracted 4f orbitals usually promote only very weak magnetic exchange.[3] Recently, however, the advent of a small contingent of dinuclear radical-bridged lanthanide complexes has demonstrated that strong magnetic exchange can be facilitated by diffuse 2,2′-bipyrimidine$^-$ or N_2^{3-} radical units.[4,5] Indeed, we have previously reported the series of complexes $[K(18\text{-crown-}6)(THF)_2]\{[(R_2N)_2(THF)Ln]_2(\mu\text{-}\eta^2\text{:}\eta^2\text{-}N_2)\}$ (**2-Ln**; Ln = Gd^{III}, Tb^{III}, Dy^{III}, Ho^{III}, Er^{III}), where a bridging N_2^{3-} radical ligand leads to an exchange constant of $J = -27$ cm^{-1}, representing the strongest magnetic exchange coupling observed to date for a Gd^{III} compound.[5a] Importantly, the strong coupling also leads to a blocking temperature of 14 K for the Tb^{III} analogue, currently the highest for any single-molecule magnet.[5b] DFT calculations for the Gd^{III} complex suggest that the coupling interaction is a result of overlap of the lanthanide 4f orbitals with the N_2^{3-} ligand orbitals, and thus, as the

Received: December 6, 2013
Published: February 28, 2014

   dx.doi.org/10.1021/ic4030102 | *Inorg. Chem.* 2014, 53, 3099−3107

Table 1. Crystal Data and Structure Refinement Parameters for 1-Ln

	1-Gd·0.5(C_7H_8)	1-Tb·0.5(C_7H_8)	1-Dy·0.5(C_6H_{14})
empirical formula	$C_{35.5}H_{92}Gd_2KN_6O_2Si_8$	$C_{35.5}H_{92}KN_6O_2Si_8Tb_2$	$C_{35}H_{95}Dy_2KN_6O_2Si_8$
fw	1213.47	1216.81	1220.98
T (K)	143(2)	143(2)	143(2)
space group	$P2_1/n$	$P2_1/n$	$P2_1/n$
a (Å)	12.4844(9)	12.4539(8)	12.4793(10)
b (Å)	21.3735(15)	21.4481(13)	21.5488(16)
c (Å)	22.3563(16)	22.3028(14)	22.2467(17)
α (deg)	90	90	90
β (deg)	104.9835(8)	104.9719(7)	105.0650(10)
γ (deg)	90	90	90
V (Å^3)	5762.6(7)	5755.1(6)	5776.8(8)
Z	4	4	4
ρ_{calcd} (Mg/m^3)	1.399	1.404	1.404
μ (mm^{-1})	2.553	2.709	2.837
R1[a] [$I > 2\sigma(I)$ = 10 615 data]	0.0250	0.0252	0.0389
wR2[b] (all data, 0.78 Å)	0.0618	0.0585	0.0826

[a]$R1 = \Sigma||F_o| - |F_c||/\Sigma|F_o|$. [b]$wR2 = [\Sigma[w(F_o^2 - F_c^2)^2]/\Sigma[w(F_o^2)^2]]^{1/2}$.

dihedral angle between the lanthanide and radical ligand deviates from planarity, the strength of the coupling is predicted to decrease.[6]

As a probe of this computational result, we set out to synthesize and structurally characterize $[\{(R_2N)_2(THF)Ln\}_2(\mu_3\text{-}\eta^2\text{:}\eta^2\text{:}\eta^2\text{-}N_2)K]$ (**1-Ln**; Ln = Gd^{III}, Tb^{III}, Dy^{III}), to determine the effects of the unsolvated K^+ counterion on the magnetism. **1-Ln** was previously reported only for diamagnetic Y^{III}: **1-Y** could be isolated following crystallization from toluene in the absence of 18-crown-6 and coordinating solvent.[7] X-ray structural characterization revealed that interaction of the K^+ ion with the N_2^{3-} radical leads to a folding of the planar Ln_2N_2 unit present in the $[K(18\text{-crown-}6)(THF)_2]^+$ salt.[8] Here, we show that this synthetic methodology can be extended to analogous complexes featuring the paramagnetic lanthanide centers Ln = Gd^{III}, Tb^{III}, and Dy^{III}. Notably, the isolation of these compounds in pure form is facilitated through utilization of an external $Nd_2Fe_{13}B$ magnet during crystal growth. Full magnetic characterization of the series reveals non-negligible antiferromagnetic coupling between the Ln^{III} centers in addition to antiferromagnetic Ln^{III}–N_2^{3-} coupling, which leads to significantly lower magnetic relaxation barriers and blocking temperatures for **1-Tb** and **1-Dy**.

EXPERIMENTAL SECTION

All syntheses and manipulations described below were conducted under nitrogen with rigorous exclusion of air and water using glovebox, Schlenk, and high-vacuum line techniques. Solvents were sparged with UHP argon and dried over columns containing Q-5 and molecular sieves. Potassium was washed with hexane and scraped to provide fresh surfaces before use. The compounds $[(R_2N)_2Ln(THF)]_2(\mu\text{-}\eta^2\text{:}\eta^2\text{-}N_2)$ (**3-Ln**; Ln = Tb,[9] Dy,[10] Gd[9]) were synthesized according to the literature method for the yttrium analogue.[11] KC_8 was prepared according to the literature procedure.[12] $Nd_2Fe_{13}B$ magnets were obtained from United Nuclear Scientific Equipment and Supplies. IR samples were prepared as KBr pellets and analyzed using a Varian 1000 FT-IR system. Elemental analyses were either performed on a Perkin-Elmer Series II 2400 CHNS analyzer at the University of California, Irvine, or by the Micro-Mass Facility at the University of California, Berkeley. Magnetic susceptibility measurements were performed using a Quantum Design MPMS2 SQUID magnetometer.

Magnetic Measurements. Magnetic samples were prepared by adding powdered crystalline compounds to a 7 mm diameter quartz tube with a raised quartz platform. Solid eicosane was added to cover the samples to prevent crystallite torqueing and provide good thermal contact between the sample and the cryogenic bath. The tubes were fitted with Teflon sealable adapters, evacuated on a Schenk line or using a glovebox vacuum pump, and sealed under static vacuum using an H_2/O_2 flame. Following flame sealing, the solid eicosane was melted in a water bath held at 40 °C.

Direct current magnetic susceptibility measurements were performed at temperatures ranging from 1.8 to 300 K, under applied fields of 0.1, 0.5, and 1 T. Alternating current magnetic susceptibility measurements were performed using a 4 Oe switching field over the frequency range 1−1500 Hz and a range of temperatures. All data for **1-Ln** were corrected for diamagnetic contributions from the core diamagnetism estimated using Pascal's constants to give χ_D = −0.000 651 94 emu/mol (**1-Gd**), −0.000 656 87 emu/mol (**1-Tb**), −0.000 661 81 emu/mol (**1-Dy**), and −0.000 243 06 emu/mol (eicosane). Cole−Cole plots were fitted using formulas describing χ' and χ'' in terms of frequency, constant temperature susceptibility (χ_T), adiabatic susceptibility (χ_S), relaxation time (τ), and a variable representing the distribution of relaxation times (α).[13] All data could be fitted with α values of ≤0.1, indicating a narrow distribution of relaxation processes.

$[\{(R_2N)_2(THF)Tb\}_2(\mu_3\text{-}\eta^2\text{:}\eta^2\text{:}\eta^2\text{-}N_2)K]$ (1-Tb). This compound was synthesized by modification of a previously reported procedure.[11] **3-Tb** (300 mg, 0.27 mmol) was dissolved in 12 mL of THF in a nitrogen-filled glovebox to afford a pale blue solution, which was stored at −30 °C for ∼1 h. A suspension of KC_8 (54 mg, 0.40 mmol) in 3 mL of THF, that was also stored at −30 °C for approximately 1 h prior to use, was added dropwise to the cold pale blue solution with vigorous stirring. The reaction mixture immediately became orange, and formation of black insoluble material was observed. As soon as the addition was complete, the mixture was filtered to remove the black solids, and the deep orange filtrate was concentrated to dryness under reduced pressure to yield a yellow powder. The powder was dissolved in a minimal amount of hexane in a vial which had a grade N45 United Nuclear $^3/_4$ in. × $^3/_4$ in. × $^1/_8$ in. $Nd_2Fe_{13}B$ plate magnet attached to the outer wall using a rubber band. After 24 h at −30 °C, green crystals (230 mg, 73%) of **1-Tb** suitable for X-ray analysis grew on the side of the vial directly in contact with the magnet as well as on the bottom of the vial. IR: 2948s, 2895m, 1441w, 1245s, 994s, 867s, 832s, 770m, 751m, 663m, 606m, 547s cm^{-1}. Anal. Calcd for $C_{32}H_{88}KN_6O_2Si_8Tb_2$·$0.5C_6H_{14}$ (**1-Tb**·$0.5C_6H_{14}$): C, 34.60; H, 7.97; N, 6.92. Found: C, 34.18; H, 7.98; N, 6.61.

$[\{(R_2N)_2(THF)Dy\}_2(\mu_3\text{-}\eta^2\text{:}\eta^2\text{:}\eta^2\text{-}N_2)K]$ (1-Dy). Following the procedure for **1-Tb**, **3-Dy** (300 mg, 0.26 mmol) was dissolved in 12 mL of THF to afford a green solution, which was treated with a KC_8 (50 mg, 0.37 mmol) suspension at −30 °C. After the mixture was filtered, removal of solvent from the red-orange filtrate afforded an orange powder, which was dissolved in a minimal amount of hexane for

dx.doi.org/10.1021/ic4030102 | Inorg. Chem. 2014, 53, 3099−3107

Scheme 1. Synthesis of the N_2^{3-} Radical-Bridged Complexes 1-Ln, Featuring an Inner-Sphere K^+ Counterion

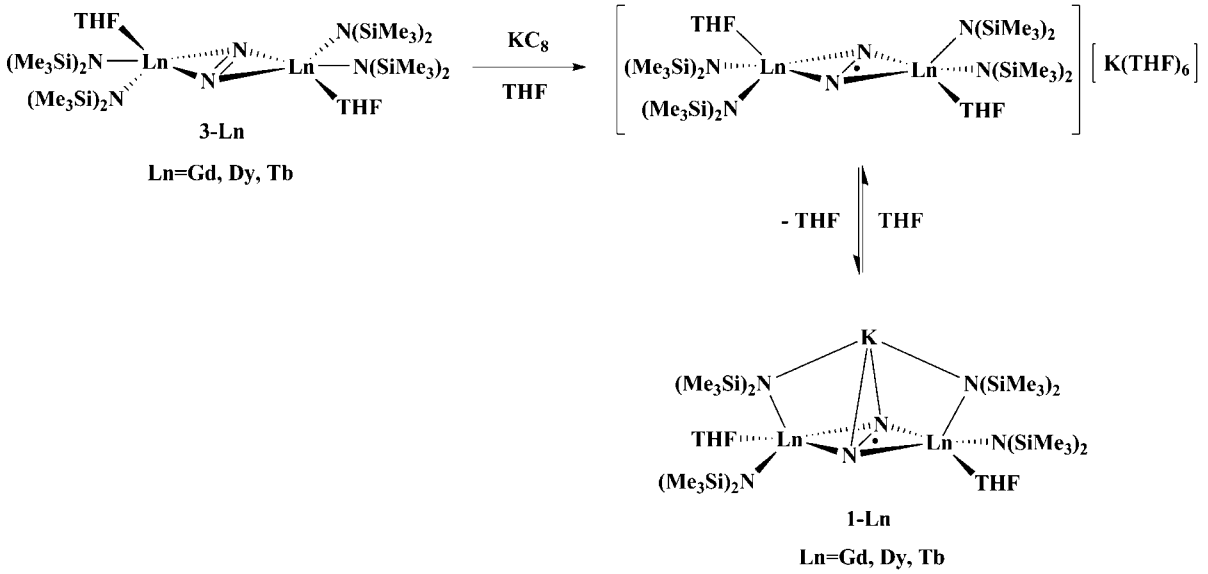

crystallization in the presence of the $Nd_2Fe_{13}B$ magnet. After 48 h at −30 °C, orange crystals (220 mg, 71%) of **1-Dy** suitable for X-ray analysis were obtained on the side of the vial directly in contact with the magnet and on the bottom of the vial. IR: 2946s, 2895s, 1443w, 1247s, 1001m, 876m, 841m, 769m, 750m, 663m, 548m cm^{-1}. Anal. Calcd for $C_{32}H_{88}KN_6O_2Si_8Dy_2{\cdot}0.5C_6H_{14}$ (**1-Dy**·$0.5C_6H_{14}$): C, 34.40; H, 7.92; N, 6.88. Found: C, 34.38; H, 8.18; N, 6.74.

[{$(R_2N)_2$(THF)Gd}$_2$(μ_3-η^2:η^2:η^2-N_2)K] (1-Gd). Following the procedure for **1-Tb**, **3-Gd** (300 mg, 0.27 mmol) was dissolved in 12 mL of THF to afford an aqua blue solution that was treated with a KC_8 (53 mg, 0.40 mmol) suspension at −30 °C. After the mixture was filtered, removal of solvent from the dark orange filtrate afforded a yellow-orange powder, which was dissolved in a minimal amount of pentane and crystallized in a vial with a $Nd_2Fe_{13}B$ magnet attached to the side. After 24 h at −30 °C, orange X-ray quality crystals of **1-Gd** (120 mg, 38%) were obtained on the side of the vial directly in contact with the magnet and on the bottom of the vial. IR: 2947s, 2895s, 1442w, 1245s, 1010m, 869m, 767m, 751m, 663m, 603m, 538m cm^{-1}. Anal. Calcd for $C_{32}H_{88}KN_6O_2Si_8Gd_2{\cdot}0.5C_5H_{12}$ (**1-Gd**·$0.5C_5H_{12}$): C, 34.70; H, 7.99; N, 6.94. Found: C, 34.64; H, 7.63; N, 7.06.

X-ray Data Collection, Structure Determination, and Refinement. Crystallographic information for complexes **1-Tb**, **1-Dy**, and **1-Gd** is summarized in Table 1 and further details can be found in the Supporting Information.

RESULTS AND DISCUSSION

Synthesis. The N_2^{3-} radical-bridged complexes **1-Ln** were synthesized by routes analogous to the one previously established for Y^{III}, as presented in Scheme 1.[7] Here, potassium graphite reduction of the corresponding neutral (N_2^{2-})-bridged complexes [$(R_2N)_2$(THF)Ln]$_2$(μ-η^2:η^2-N_2), **3-Ln**,[9,10] followed by filtration and removal of THF, yielded the desired products as yellow or orange powders. If left at room temperature, these powders will decompose to form pale products within 24 h, though they are stable when stored at −30 °C. Crystallization of the isolated powders from toluene at −30 °C leads to a mixture of crystals of **1-Ln** and the neutral (N_2^{2-})-bridged complex, **3-Ln**, as determined by X-ray crystallography. ^{1}H NMR spectroscopy on isolated samples of **1-Y** show decomposition to **3-Y** occurs within hours in solution.

It was subsequently found that using excess KC_8 in the reduction of [$(R_2N)_2$(THF)Ln]$_2$(μ-η^2:η^2-N_2) gave samples of **1-Ln** with higher purity. While excess KC_8 was previously avoided owing to its potential for degrading the reduced product,[7] it can evidently be tolerated in the short reaction times used here. This is consistent with the sensitive nature of this multicomponent reduction system, where the reaction rates, order of KC_8 addition, and reaction concentration are all important variables.[7] A combination of short reaction times with excess KC_8 and crystallizations in the presence of a $Nd_2Fe_{13}B$ magnet (*vide infra*) produced pure crystals of **1-Ln** suitable for magnetic studies.

Crystallization Using a $Nd_2Fe_{13}B$ Magnet. Due to the difficulty encountered in isolating pure **1-Ln** using standard recrystallization techniques, alternative routes to purification were investigated. Notably, the use of magnetic fields to effect the separation of various materials has been well-established since the 1960s and 1970s,[14] largely tailored toward mineralogical applications. Magnetic fields produced by rare earth magnets have more recently been employed in many other applications, such as iron ore refinement[15] and water purification,[16] and on a laboratory scale in the fractionation and manipulation of magnetic nanoparticles.[17] An extensive body of work also exists on the use of magnetic levitation (MagLev) for the separation of various diamagnetic materials. In this technique, diamagnetic substances are placed in an aqueous paramagnetic solution that is then positioned between two $Nd_2Fe_{13}B$ magnets with like poles facing.[18] Materials are separated within the solution based on a balance between their magnetic susceptibilities and their differing densities. MagLev has very recently been extended to address the often difficult task of separating diamagnetic crystal polymorphs.[19]

Considering these results, we sought to purify the highly anisotropic paramagnetic **1-Ln** with the aid of a strong external $Nd_2Fe_{13}B$ magnet. To our knowledge, rare earth magnets have not previously been reported to effect the crystallization of paramagnetic molecules in solution. Such a technique would rest on the fact that paramagnetic molecules will be much more strongly attracted to a magnet than say, diamagnetic impurities, or less paramagnetic substances (e.g., complexes with smaller spin). A magnet-driven concentration gradient in solution should thus lead to more rapid and preferential crystallization of the most paramagnetic substance. Indeed, it was found that crystals of **1-Ln** could be cleanly and swiftly crystallized without

dx.doi.org/10.1021/ic4030102 | Inorg. Chem. 2014, 53, 3099−3107

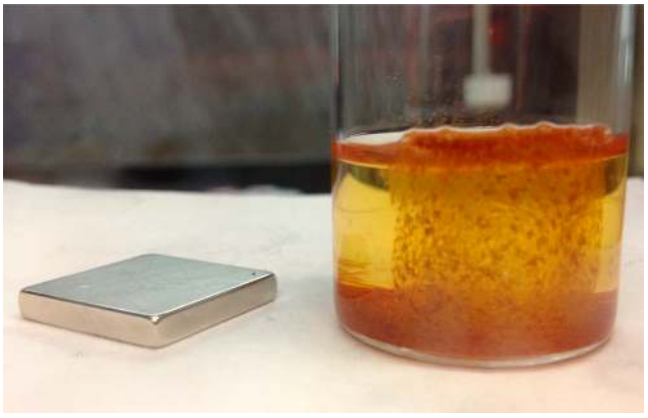

Figure 1. Crystals of **1-Dy** grown with the aid of a $Nd_2Fe_{13}B$ magnet. A cluster of crystals can be seen along the side of the vial in a square formation where the magnet was attached to the outer wall.

accompanying formation of **3-Ln** by positioning a $Nd_2Fe_{13}B$ magnet adjacent to the crystallization vessel (Figure 1). While crystals also grow elsewhere in the vial, the majority are observed to form on the wall to which the magnet is attached. What is fascinating to note is that, in some cases, the individual crystallites seem to form in a pattern defined by magnetic field lines (see Figure 1 and Supporting Information Figure S7).

Among **1-Ln**, this effect is most pronounced for Dy and Tb (Supporting Information Figure S1), with less efficient crystal growth observed for the magnetically isotropic Gd complex (Supporting Information Figure S2). The effect is not noticeable for **1-Y** (Supporting Information Figure S3), which has only one unpaired electron per molecular unit. Given the greater impact on crystallization noted for **1-Tb** and **1-Dy** over **1-Gd**, this effect seems to be strongly correlated with large anisotropy, concentration, and a high number of unpaired electrons. It is likely, however, that this technique is most useful in enhancing the rate of crystallization for the present complexes, as opposed to selectively crystallizing **1-Ln** from **3-Ln**. Such a conclusion is rationalized by the fact that magnet-induced crystal growth was also found to occur readily for **3-Tb** and **3-Dy** (Supporting Information Figures S4 and S5). However, this technique should generally be useful in the efficient crystallization and separation of other highly paramagnetic complexes (see Supporting Information Figures S6–S8) from diamagnetic or less paramagnetic molecular species in solution.

X-ray Crystallographic Studies. Complexes **1-Ln** crystallize in the monoclinic space group $P2_1/n$ and are isomorphous with the previously reported Y^{III} analogue (Figure 2).[7] In the absence of coordinating solvent or other encapsulating agents, the K^+ cation is found above the N_2^{3-} bridge, and the N atoms of two NR_2 ligands orient inward to form a dative interaction with the metal cation. The K–N distances involving the N_2^{3-} bridge are 2.844(3)–2.888(2) Å, close to those of **1-Y** and at the long end of the 2.714(6)–2.800(6) Å range observed for other K–(η^2-N_2) distances in the literature.[20−22] The distances of 2.959(2)–2.988(3) Å for K–N(NR_2) are much longer than the 2.760(1) Å K–N distance in (18-crown-6)K(NR_2),[23] as expected, and are similar to the 2.908 Å bridging K–N[μ-NR_2] distance in $[(R_2N)Sm(\mu\text{-}NR_2)_2K]_n$.[24]

A comparison of the metrical parameters for **1-Ln** and **2-Ln** (Table 2) reveals the N–N distances within the N_2^{3-} radical bridges to be the same within error, and the Ln–N(NR_2) distances to decrease slightly as a function of ionic radii (in the order Gd > Tb > Dy). The Ln–O(THF) distances of **1-Ln** are slightly shorter than those of **2-Ln**, which could be due to a decrease in steric interactions of the ligands as the amides orient toward the inner sphere K^+ ion in **1-Ln**. The most notable structural change in **1-Ln** is a folding of the previously planar Ln_2N_2 core unit found in **2-Ln** to generate dihedral angles between the two LnN_2 planes of 13.64° in **1-Gd**, 16.12° in **1-Tb**, and 15.27° in **1-Dy**.

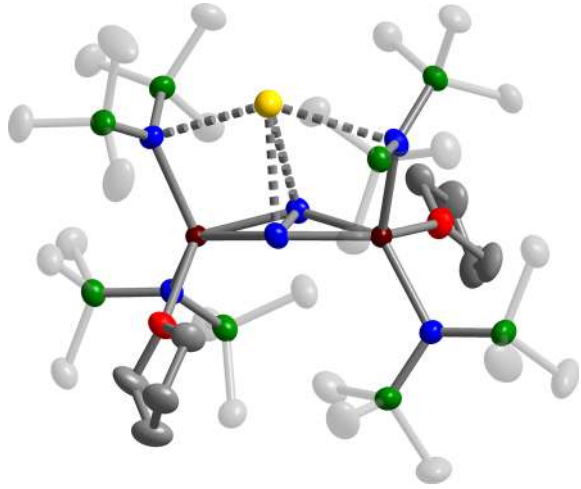

Figure 2. Structure of the N_2^{3-} radical-bridged complex **1-Tb**, with thermal ellipsoids drawn at the 70% probability level. Dark red, blue, green, red, gray, and yellow ellipsoids represent Tb, N, Si, O, C, and K atoms, respectively. Hydrogen atoms have been omitted for clarity.

Static Magnetic Susceptibility Measurements. Temperature-dependent dc magnetic susceptibility measurements were carried out for complexes **1-Ln** between 1.8 and 300 K at fields of 0.1 or 1 T. Comparison of the values of $\chi_M T$ versus T for **1-Ln** with data previously reported for the **2-Ln**[5] complexes without inner sphere K^+ ions reveals stark differences in the magnetism of the two series (Figure 3). For **1-Gd** (Figure 3a, green circles), $\chi_M T$ is 16.28 emu K/mol at 300 K, larger than that observed for **2-Gd** (15.25 emu K/mol)[5b] and corresponding to the value of 16.31 emu K/mol expected for two uncoupled $S = {}^7/_2$ Gd^{III} centers and an $S = {}^1/_2$ radical bridge. A shallow minimum occurs at 185 K upon lowering the temperature, significantly below the temperature of >300 K for **2-Gd**,[5b] but greater than the 135 K minimum observed for the bipyrimidine radical-bridged species $\{[(C_5Me_5)_2Gd]_2(\mu\text{-bpym}^{\bullet})\}^+$.[4] The susceptibility reaches a maximum of 18.25 emu K/mol at 18 K for **1-Gd**, which is much lower than the maximum of 23.83 emu K/mol occurring for **2-Gd** at 9 K. The latter corresponds well to the value of 24.38 emu K/mol expected for an $S = {}^{13}/_2$ ground state arising from strong antiferromagnetic exchange between Gd^{III} and the N_2^{3-} radical bridge.[5a]

In contrast, the $\chi_M T$ maximum for **1-Gd** is closer to the expected value for an $S = {}^{11}/_2$ ground state (17.88 emu K/mol), which is not reasonable assuming simple antiferromagnetic coupling between the Gd^{III} centers and the N_2^{3-} radical bridge. Another distinct feature in the $\chi_M T$ data for **1-Gd** is the presence of a downturn following the maximum at 18 K, which might be attributed to the presence of competing exchange interactions.[25]

With its half-filled 4f shell, Gd^{III} possesses no orbital angular momentum, thus enabling analysis of its magnetic behavior

dx.doi.org/10.1021/ic4030102 | Inorg. Chem. 2014, 53, 3099–3107

Table 2. Selected Interatomic Distances (Å) and Angles (deg) for {[$(R_2N)_2(THF)Ln]_2(\mu$-η^2:η^2-$N_2)$}K (1-Ln) and [K(18-crown-6)$(THF)_2$]{[$(R_2N)_2(THF)Ln]_2(\mu$-η^2:η^2-$N_2)$} (2-Ln)

	N−N (Å)	K−N(N_2^{3-}) (Å)	K−(NR_2) (Å)	Ln−(NR_2) (Å)	Ln−O (Å)	Ln−N−N−Ln dihedral angle (deg)
1-Gd	1.395(3)	2.875(2)	2.959(2)	2.354(2)	2.425(2)	13.64
		2.888(2)	2.971(2)	2.378(2)		
2-Gd	1.401(4)			2.357(2)	2.480(2)	0
				2.382(2)		
1-Tb	1.401(3)	2.844(3)	2.977(3)	2.337(2)	2.413(2)	16.12
		2.868(3)	2.988(3)	2.358(2)		
2-Tb	1.394(3)			2.331(2)	2.479(1)	0
				2.360(2)		
1-Dy	1.404(5)	2.852(4)	2.968(4)	2.324(4)	2.392(3)	15.27
		2.870(4)	2.980(4)	2.347(4)		
2-Dy	1.399(2)			2.314(1)	2.455(1)	0
				2.343(1)		

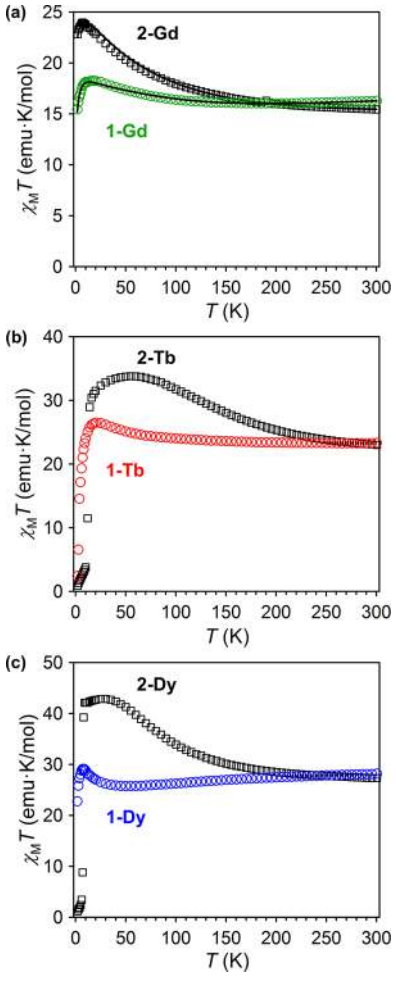

Figure 3. Plot of the molar magnetic susceptibility times temperature ($\chi_M T$) versus T for **1-Ln** (colored circles) and **2-Ln** (black squares). Data for the Gd^{III} and Dy^{III} complexes were collected under H_{dc} = 0.1 T, while data for **1-Tb** was collected under H_{dc} = 1 T to compare with the previously reported literature data for **2-Tb**. Fits using the Hamiltonians described in the text are represented by black lines. For **1-Gd**, a good fit to the data is achieved by considering intramolecular Gd^{III}−(N_2^{3-}) and Gd^{III}−Gd^{III} coupling, resulting in $J = -27.1(4)$ cm^{-1} and $J' = -2.28(1)$ cm^{-1}, respectively, with g = 2.17. When the data for **1-Gd** is adjusted for a mass error of ∼2 mg, g = 2.09, while the values of J and J' do not change within error, thus the larger g-value obtained from fitting is likely the result of a small mass error.

using a standard spin-only model. In order to quantify the difference in exchange coupling between **1-Gd** and **2-Gd**, we set out to model the magnetic susceptibility data of the former using the isotropic Heisenberg−Dirac−Van Vleck Hamiltonian $\hat{H} = -2J\hat{S}_{radical}\cdot(\hat{S}_{Gd1} + \hat{S}_{Gd2})$. Assuming all coupling interactions are accounted for, such a spin-only Hamiltonian represents a reasonable model for complexes containing paramagnetic centers with no orbital angular momentum, such as $^8S_{7/2}$ Gd^{III} and an $S = {}^1/_2$ N_2^{3-} radical bridge. However, use of this Hamiltonian resulted in a satisfactory fit of the experimental data only above 40 K. Addition of a second term accounting for a weak intermolecular interaction[5a] still did not enhance the fit below 40 K. We considered that, owing to the nonzero dihedral angle between the two GdN_2 planes present in **1-Gd**, intramolecular Gd^{III}−Gd^{III} coupling might also contribute to the overall magnetic susceptibility, and therefore, the system would be better modeled as a triangle of paramagnetic centers with $(N_2)^{3-}$ at the apex. This scenario can be described by the Hamiltonian $\hat{H} = -J(\hat{S}_{radical}\cdot\hat{S}_{Gd1} + \hat{S}_{radical}\cdot\hat{S}_{Gd2}) - J'(\hat{S}_{Gd1}\cdot\hat{S}_{Gd2})$,[26] where J represents the coupling between a Gd^{III} center and the N_2^{3-} radical, while J' quantifies the intramolecular coupling between the two Gd^{III} centers. With the inclusion of a very small intermolecular coupling constant of $J'' = 0.020(1)$ cm^{-1}, this model provides a good fit to the magnetic susceptibility data over the entire temperature range 1.8−300 K yielding $J = -27.1(4)$ cm^{-1} and $J' = -2.28(1)$ cm^{-1} (Figure 3a). The improvement in the fit (largely below 40 K) with the inclusion of this intramolecular term indicates that the coupling between Gd^{III} centers is significant only below this temperature,[27] and therefore, such an interaction is also likely to influence the magnetic relaxation behavior of **1-Tb** and **1-Dy**.

Notably, the Gd^{III}−(N_2^{3-}) coupling constant obtained for **1-Gd** matches the value of $J = -27$ cm^{-1} previously reported for **2-Gd**.[5a] Thus, the small bend in the Gd^{III}−(N_2^{3})$^-$−Gd^{III} unit appears to have little impact on the strength of the Gd^{III}−(N_2^{3-}) coupling. Indeed, DFT calculations predicted that this coupling strength should decrease by only ∼5 cm^{-1} with a dihedral angle of 13.5°.[6] A less intuitive result of fitting the dc susceptibility data is the occurrence of significant exchange coupling directly between the Gd^{III} centers, which was not necessary to include in modeling the data for **2-Gd**, and was predicted by DFT calculations[6] to be just −0.5 cm^{-1}. While literature data are somewhat sparse for exchange coupling between Gd^{III} centers, the magnitude of the experimental value of −2.28(1) cm^{-1} dwarfs recently reported values for antiferromagnetic superexchange mediated by semiquinone

dx.doi.org/10.1021/ic4030102 | Inorg. Chem. 2014, 53, 3099−3107

radical,[28] phenoxylate,[29] or carboxylate[30] bridges. Much work has also been done to characterize the nature of the magnetic coupling in Ln^{III} nitronyl nitroxide chains,[31] and notably, in some cases, antiferromagnetic next-nearest-neighbor Gd^{III}–Gd^{III} exchange has been observed that is even stronger than the metal–radical exchange interaction, on the order of $J = -0.98$ cm^{-1}.[31c,f] Very recently, a comparable antiferromagnetic exchange interaction with $J = -1.22$ cm^{-1} has also been shown between Gd^{III} ions bridged by hydride ligands, where the $Gd^{III}\cdots Gd^{III}$ separation is 3.4140(6) Å.[32] Given the large separation of 4.267 Å between Gd^{III} centers in **1-Gd**, we surmise that the mechanism here is most likely via superexchange through the N_2^{3-} ligand. For comparison, an exchange constant of $J = -0.49$ cm^{-1} was observed for the planar (N_2^{2-})-bridged species **3-Ln**[5a] indicating that the strength of the exchange increases considerably upon reduction of the bridging intermediary to N_2^{3-} and folding of the Gd_2N_2 core unit.

The competing Gd^{III}–Gd^{III} exchange interaction that arises in **1-Gd** has a dramatic effect on its magnetic susceptibility data, as manifested in a suppression of the magnetic moment at low temperatures (see Figure 3a). The origin of this effect is apparent upon comparing plots of the spin state energy level structures obtained from fits to the susceptibility data, as shown in Figure 4. Here, the simple level ordering of **2-Gd** expected

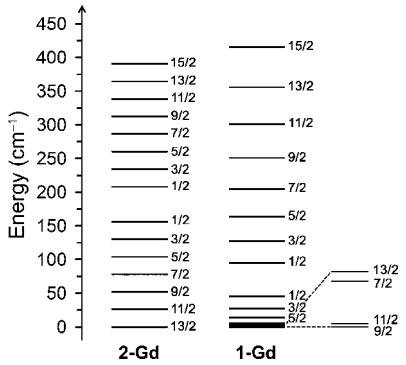

Figure 4. Spin state energy level diagrams for **2-Gd** and **1-Gd** as obtained from fitting using the Hamiltonians described in the text and in ref 5a. For **2-Gd**, antiferromagnetic coupling between the Gd^{III} centers and the N_2^{3-} radical bridge gives rise to a ground state of $S = {}^{13}/_2$. In contrast, competing antiferromagnetic coupling between the Gd^{III} centers in **1-Gd** results in an $S = {}^9/_2$ ground state that is nearly degenerate with the first excited state of $S = {}^{11}/_2$.

for strong antiferromagnetic exchange between an $S = {}^1/_2$ radical and two $S = {}^7/_2$ Gd^{III} centers is disrupted by the antiferromagnetic Gd^{III}–Gd^{III} exchange. Namely, whereas the $S = {}^{13}/_2$ ground state of **2-Gd** is well-isolated from an $S = {}^{11}/_2$ excited state, for **1-Gd** the ground state is a lower spin $S = {}^9/_2$ state that is separated by only 0.29 cm^{-1} from an $S = {}^{11}/_2$ excited state. Variable-field magnetization measurements performed at low temperature up to 7 T for **1-Gd** confirm the calculated $S = {}^9/_2$ ground state (Supporting Information Figure S9). At temperatures of 2, 4, and 6 K, the $M(H)$ curves for **1-Gd** exactly overlay with the Brillouin curves expected for an $S = {}^9/_2$ system until fields beyond 1 T, when the experimental curve passes through $S = {}^{11}/_2$ (at ~3.5 T) before meeting with $S = {}^{13}/_2$.

Direct current magnetic susceptibility measurements performed on **1-Tb** and **1-Dy** reveal similar trends to those observed for **1-Gd** (Figure 3b,c, colored circles). While significant magnetic anisotropy for **1-Tb** and **1-Dy** precludes fitting of the $\chi_M T$ data using a spin-only approximation, the general results obtained for **1-Gd** may be extended to gain a qualitative understanding of the magnetism. In particular, we would anticipate for these compounds that the moment of the ground state is reduced as a result of antiferromagnetic Tb^{III}–Tb^{III} and Dy^{III}–Dy^{III} exchange interactions. At room temperature, the $\chi_M T$ values for **1-Tb** and **1-Dy** are 23.77 and 28.17 emu K/mol, very close to those expected for two uncoupled Ln^{III} centers and an $S = {}^1/_2$ radical (24.0 and 28.7 emu K/mol, respectively). Maxima in $\chi_M T$ are encountered for **1-Tb** and **1-Dy** at temperatures of 10 and 8 K, respectively, with corresponding $\chi_M T$ values of 28.44 and 29.12 emu K/mol. These maxima are much less than those for **2-Tb** and **2-Dy** at 33.76 emu K/mol and 42.54 emu K/mol, consistent with competing antiferromagnetic interactions between Ln^{III} centers, as observed in **1-Gd**. One also observes an extraordinary suppression in the magnitudes of the magnetic moments for **1-Tb** and **1-Dy** compared to the parent complexes **2-Tb** and **2-Dy** (Figures 3b,c, black squares), again highlighting the impact of Ln^{III}–Ln^{III} coupling upon bending of the Ln_2N_2 core unit. Considering just the susceptibility behavior of **1-Ln**, the $\chi_M T$ maximum for **1-Tb** hints at stronger magnetic coupling relative to **1-Dy**, an observation supported by the temperature-dependence of $\chi_M T$ below these maxima. For **1-Tb**, $\chi_M T$ falls abruptly to a final value of 4.71 emu K/mol at 1.8 K, while a very small decline in the case of **1-Dy** yields a value of $\chi_M T$ = 22.75 emu K/mol at the same temperature. The sharp decline for **1-Tb** is indicative of magnetic blocking; however, the same phenomenon is lacking for **1-Dy** in the range of temperatures accessible by our magnetometer, indicating the latter has a much lower blocking temperature.

Dynamic Magnetic Susceptibility Measurements. To probe for slow relaxation of the magnetization, ac magnetic susceptibility data were collected for **1-Tb** and **1-Dy** over a range of temperatures using a 4 Oe switching field and frequencies from 1 to 1500 Hz. An out-of-phase signal (χ_M'') is observed under zero applied field for both complexes (Figure 5, upper, and Supporting Information Figure S10), although at much lower temperatures and over a narrower range than previously observed for **2-Tb** and **2-Dy**.[5] Relaxation times (τ) were extracted for **1-Tb** and **1-Dy** at the various temperatures by fitting the frequency-dependent χ_M' and χ_M'' data using a generalized Debye model.[13] Small values of the alpha (α) parameter ($\leq$0.1) revealed the relaxation to be uniform over the temperature and frequency range probed.

Indeed, a plot of the natural logarithm of τ versus $1/T$ is linear for **1-Tb** and **1-Dy**; thus, relaxation occurs predominantly through a thermally activated Orbach process.[33] Fitting to an Arrhenius-type activation law yields barriers of U_{eff} = 41.13(4) cm^{-1} for **1-Tb** and 14.95(8) cm^{-1} for **1-Dy** (Figure 5, lower), significantly reduced from those of the parent outer-sphere complexes at 227.0(4) cm^{-1} (**2-Tb**)[5b] and 123 cm^{-1} (**2-Dy**),[5a] though within range of many terbium and dysprosium single-molecule magnets described in the literature.[1f] The much faster relaxation and smaller barriers observed for both compounds are a direct testimony to the influence of the competing antiferromagnetic coupling interaction on the energy landscape. Additionally, while **2-Tb** and **2-Dy** both possess τ_0 values on the order of 10^{-9} s,[5] corresponding well to pure Orbach relaxation, τ_0 values of $3.89(2) \times 10^{-6}$ and $3.2(1) \times 10^{-7}$ s for **1-Tb** and **1-Dy**, respectively, suggest that additional relaxation

dx.doi.org/10.1021/ic4030102 | Inorg. Chem. 2014, 53, 3099–3107

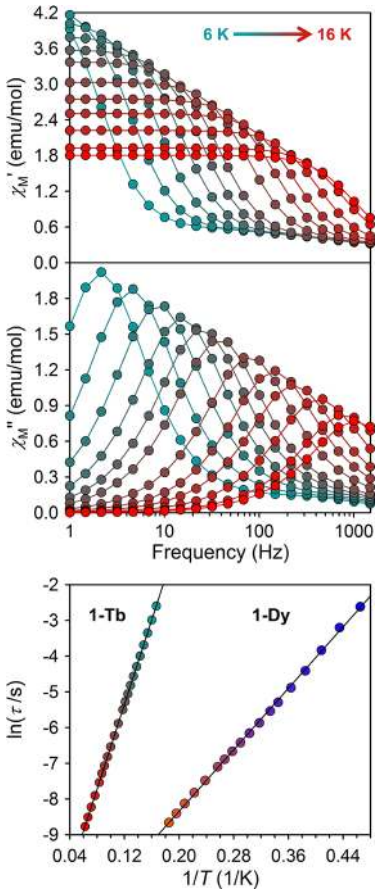

Figure 5. Upper: Plot of the molar in-phase (χ_M') and out-of-phase (χ_M'') magnetic susceptibility versus frequency of the oscillating field for **1-Tb** over the temperature range 6−16 K and frequencies between 1 and 1500 Hz under zero-applied dc field. Lower: Plot of the natural log of the relaxation time, ln(τ), versus $1/T$ for **1-Tb** and **1-Dy** under zero applied dc field. Black lines represent fits to the Arrhenius expression $\ln(\tau) = \ln(\tau_0) + U_{eff}/k_BT$ yielding U_{eff} = 41.13(4) cm^{-1}/τ_0 = 3.89(2) × 10^{-6} s (**1-Tb**) and U_{eff} = 14.95(8) cm^{-1}/τ_0 = 3.2(1) × 10^{-7} s (**1-Dy**).

mechanisms may be active at the temperatures and frequencies probed. At high ac frequencies, such a conclusion is also supported by an additional small increase in χ_M'' for both complexes and the nonzero value of χ_M' for **1-Tb**.

While the relaxation time for **1-Dy** is still within the ac frequency range near the lowest temperatures accessible by our SQUID magnetometer, ac relaxation for **1-Tb** is only apparent above 6 K. In order to probe relaxation at lower temperatures, variable-field magnetization measurements were carried out from 1.8 K at a sweep rate of 1 mT/s. As anticipated, an open magnetic hysteresis loop is observed for **1-Tb**, which remains open to temperatures as high as 3.8 K (Figure 6). This maximum hysteresis temperature is only a fraction of that observed for **2-Tb** at 14 K,[5b] again emphasizing the lower moment and weaker overall coupling engineered by the bridging K$^+$ counterion in **1-Tb**.

An interesting feature in the magnetic hysteresis of **1-Tb**, not observed for **2-Tb**, is the presence of two steps, one centered at zero field for all temperatures. Such drops in the magnetization indicate rapid relaxation, often ascribed to tunneling of the magnetization.[34] Indeed, the energy separation between ground and first excited S in **1-Gd** (0.29 cm^{-1}) is on the order of the tunnel splitting in some molecular magnets.[35] A similar

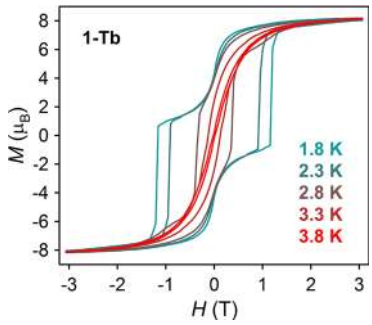

Figure 6. Variable-field magnetization for **1-Tb** collected at a sweep rate of 1 mT/s. At 1.8 K, the remnant magnetization and coercive field are 4.28 μ_B and 1.1 T.

separation between ground and excited M_J states for **1-Tb**, generated in the presence of low temperature Tb^{III}−Tb^{III} exchange, could be considered an effective tunnel splitting, promoting tunneling and hence a magnetization drop at zero field. Another possibility is the presence of non-negligible dipolar interactions, which could create a small bias and allow for tunneling at zero field.

Field-dependent ac susceptibility scans suggest[36] that the second, much more drastic magnetization drop is mediated by resonant tunneling of the magnetization, a possibility that could again be rationalized by considering the energy landscape determined for **1-Gd** as a model. Given the presence of a few closely-spaced excited states in **1-Ln** (spanning ~5 cm^{-1} for **1-Gd**) arising from the competing Ln^{III}−Ln^{III} exchange, for the anisotropic lanthanide ions resonant M_J states are more likely to occur than in **2-Ln**, where strong concerted exchange effects a much greater separation between ground and first excited state (see Supporting Information Table S1).[37] Other possible mitigating factors such as dipolar interactions or the occurrence of a magnetic avalanche cannot be dismissed, however. Due to the potential relevance of dipolar interactions in promoting tunneling[34] and magnetic avalanches,[38] we made several attempts to characterize dilute solution samples prepared in both toluene and 2-methyltetrahydrofuran glasses. However, **1-Tb** was found to decompose rapidly in these solutions, precluding further characterization. Ultimately, detailed theoretical analysis will be necessary to validate any of these interpretations and fully understand the magnetic hysteresis behavior.

■ CONCLUSIONS

The compounds [{(R$_2$N)$_2$(THF)Ln}$_2$(μ_3-η^2:η^2:η^2-N$_2$)K], **1-Ln**, with Ln = Gd, Tb, and Dy, featuring an inner-sphere K$^+$ counterion, were synthesized for comprehensive magnetic comparison with the previously reported single-molecule magnets [K(18-crown-6)(THF)$_2$]{[(R$_2$N)$_2$(THF)Ln]$_2$(μ-η^2:η^2-N$_2$)}, **2-Ln**. Compounds **1-Ln** are less thermally stable than **2-Ln** and require shorter periods of crystallization before partial decomposition to products such as the N$_2^{2-}$ starting materials [(R$_2$N)$_2$Ln(THF)]$_2$(μ-η^2:η^2-N$_2$), **3-Ln**. Isolation of pure **1-Ln** was found to be significantly aided by crystal growth in the presence of a Nd$_2$Fe$_{13}$B magnet adjacent to the crystallization vial, with **1-Ln** crystals forming predominantly on the side of the vial where the magnet was attached. This technique is not limited to radical-bridged dinuclear species, and has been found to be advantageous in promoting the

dx.doi.org/10.1021/ic4030102 | Inorg. Chem. 2014, 53, 3099−3107

crystallization of other complexes with large moments and anisotropy.

The compounds **1-Tb** and **1-Dy** are single-molecule magnets like the parent **2-Tb** and **2-Dy** compounds, but exhibit shorter relaxation times and much smaller relaxation barriers. Fitting of static magnetic susceptibility data for **1-Gd** reveals strong antiferromagnetic $Gd^{III}-(N_2^{3-})$ radical coupling that is the same strength as in the parent compound **2-Gd**, with $J \sim -27$ cm^{-1}. However, folding of the $Gd^{III}-(N_2^{3-})-Gd^{III}$ unit also introduces a small antiferromagnetic coupling interaction directly between Gd^{III} centers, which competes with the parallel alignment of Gd^{III} spins enforced by the antiferromagnetic $Gd^{III}-(N_2^{3-})$ radical coupling. The resulting energy spectrum of **1-Gd** consists of an $S = {}^{9}/_{2}$ ground state with a low-lying $S = {}^{11}/_{2}$ excited state, and it is this absence of a well-isolated, higher-moment ground state that is likely the source of faster relaxation and smaller blocking temperatures for **1-Tb** and **1-Dy**. These results reveal the importance of a planar $Ln^{III}-(N_2^{3-})-Ln^{III}$ unit to strong concerted exchange and very slow magnetic relaxation,[5] and perhaps more importantly highlight how a simple alkali metal such as potassium can be used to dramatically affect magnetic behavior.

■ ASSOCIATED CONTENT

Supporting Information

Additional experimental details, crystallographic data collection, structure solution, and refinement (PDF) and X-ray diffraction details of compounds **1-Ln** (CIF, CCDC 975338−975340). This material is available free of charge via the Internet at http://pubs.acs.org.

■ AUTHOR INFORMATION

Corresponding Authors

*E-mail: jrlong@berkeley.edu.
*E-mail: wevans@uci.edu.

Author Contributions

[§]These two authors contributed equally to this work.

Notes

The authors declare no competing financial interest.

■ ACKNOWLEDGMENTS

We thank the National Science Foundation for support under Grants CHE-1111900 (J.R.L.) and CHE-1265396 (W.J.E.), and McDonald's Corporation for the drinking straws employed in magnetic sample loading. K.R.M. thanks Wayne W. Lukens for valuable discussions.

■ REFERENCES

(1) (a) Ishikawa, N.; Sugita, M.; Ishikawa, T.; Koshihara, S.-y.; Kaizu, Y. *J. Am. Chem. Soc.* **2003**, *125*, 8694−8695. (b) AlDamen, M. A.; Clemente-Juan, J. M.; Coronado, E.; Martí-Gastaldo, C.; Gaita-Ariño, A. *J. Am. Chem. Soc.* **2008**, *130*, 8874−8875. (c) Jiang, S.-D.; Wang, B.-W.; Sun, H.-L.; Wang, Z.-M.; Gao, S. *J. Am. Chem. Soc.* **2011**, *133*, 4730−4733. (d) Baldoví, J. J.; Borrás-Almenar, J. J.; Clemente-Juan, J. M.; Coronado, E.; Gaita-Ariño, A. *Dalton Trans.* **2012**, *41*, 13705−13710. (e) Chilton, N. F.; Langley, S. K.; Moubaraki, B.; Soncini, A.; Batten, S. R.; Murray, K. S. *Chem. Sci.* **2013**, *4*, 1719−1730. (f) Woodruff, D. N.; Winpenny, R. E.; Layfield, R. A. *Chem. Rev.* **2013**, *113*, 5110−5148.

(2) Blagg, R. J.; Ungur, L.; Tuna, F.; Speak, J.; Comar, P.; Collison, D.; Wernsdorfer, W.; McInnes, E. J. L.; Chibotaru, L. F.; Winpenny, R. E. P. *Nat. Chem.* **2013**, *5*, 673−678.

(3) Sessoli, R.; Powell, A. K. *Coord. Chem. Rev.* **2009**, *253*, 2328−2341.

(4) Demir, S.; Zadrozny, J. M.; Nippe, M.; Long, J. R. *J. Am. Chem. Soc.* **2012**, *134*, 18546−18549.

(5) (a) Rinehart, J. D.; Fang, M.; Evans, W. J.; Long, J. R. *Nat. Chem.* **2011**, *3*, 538−542. (b) Rinehart, J. D.; Fang, M.; Evans, W. J.; Long, J. R. *J. Am. Chem. Soc.* **2011**, *133*, 14236−14239.

(6) Rajeshkumar, T.; Rajaraman, G. *Chem. Commun.* **2012**, *48*, 7856−7858.

(7) Evans, W. J.; Fang, M.; Zucchi, G.; Furche, F.; Ziller, J. W.; Hoekstra, R. M.; Zink, J. I. *J. Am. Chem. Soc.* **2009**, *131*, 11195−11202.

(8) Fang, M.; Bates, J. E.; Lorenz, S. E.; Lee, D. S.; Rego, D. B.; Ziller, J. W.; Furche, F.; Evans, W. *Inorg. Chem.* **2011**, *50*, 1459−1469.

(9) Evans, W. J.; Lee, D. S.; Rego, D. B.; Perotti, J. M.; Kozimor, S. A.; Moore, E. K.; Ziller, J. W. *J. Am. Chem. Soc.* **2004**, *126*, 14574−14582.

(10) Evans, W. J.; Zucchi, G.; Ziller, J. W. *J. Am. Chem. Soc.* **2003**, *125*, 10−11.

(11) Evans, W. J.; Lee, D. S.; Ziller, J. W. *J. Am. Chem. Soc.* **2004**, *126*, 454−455.

(12) Bergbreiter, D. E.; Killough, J. M. *J. Am. Chem. Soc.* **1978**, *100*, 2126−2134.

(13) Gatteschi, D.; Sessoli, R.; Villain, J. *Molecular Nanomagnets*; Oxford University Press: Oxford, 2006.

(14) (a) Andres, U. *Magnetohydrodynamic & Magnetohydrostatic Methods of Mineral Separation*; John Wiley & Sons: New York, NY, 1976. (b) Alminas, H. V.; Marceau, T. L.; Hoffman, J. D.; Bigelow, R. C. *A Laboratory-Scale Magnetohydrostatic Separator and its Application to Mineralogic Problems*; United States Government Printing Office: Washington, DC, 1984.

(15) Arvidson, B. R.; Henderson, D. *Miner. Eng.* **1997**, *10*, 127−137.

(16) Ambashta, R. D.; Sillanpää, M. *J. Hazard. Mater.* **2010**, *180*, 38−49.

(17) Latham, A. H.; Freitas, R. S.; Schiffer, P.; Williams, M. E. *Anal. Chem.* **2005**, *77*, 5055−5062.

(18) Mirica, K. A.; Shevkoplyas, S. S.; Phillips, S. T.; Gupta, M.; Whitesides, G. M. *J. Am. Chem. Soc.* **2009**, *131*, 10049−10058 and references therein.

(19) Atkinson, M. B. J.; Bwambok, D. K.; Chen, J.; Chopade, P. D.; Thuo, M. M.; Mace, C. R.; Mirica, K. A.; Kumar, A. A.; Myerson, A. S.; Whitesides, G. M. *Angew. Chem., Int. Ed.* **2013**, *125*, 10398−10401.

(20) Yelamos, C.; Heeg, M. J.; Winter, C. H. *Inorg. Chem.* **1998**, *37*, 3892−3894.

(21) Pfirrmann, S.; Limberg, C.; Herwig, C.; Stober, R.; Ziemer, B. *Angew. Chem., Int. Ed.* **2009**, *48*, 3357−3361.

(22) Smith, J. M.; Sadique, A. R.; Cundari, T. R.; Rodgers, K. R.; Lukat-Rodgers, G.; Lachicotte, R. J.; Flaschenriem, C. J.; Vela, J.; Holland, P. L. *J. Am. Chem. Soc.* **2006**, *128*, 756−769.

(23) Evans, W. J.; Rego, D. B.; Ziller, J. W. *Inorg. Chem.* **2006**, *45*, 3437−3443.

(24) Evans, W. J.; Johnston, M. A.; Clark, R. D.; Anwander, R.; Ziller, J. W. *Polyhedron* **2001**, *20*, 2483−2490.

(25) Milios, C. J.; Gass, I. A.; Vinslava, A.; Budd, L.; Parsons, S.; Wernsdorfer, W.; Perlepes, S. P.; Christou, G.; Brechin, E. K. *Inorg. Chem.* **2007**, *46*, 6215−6217.

(26) Kahn, O. *Molecular Magnetism*; VCH Publishers, Inc.: New York, 1993.

(27) Benelli, C.; Gatteschi, D. *Chem. Rev.* **2002**, *102*, 2369−2388.

(28) Dei, A.; Gatteschi, D.; Massa, C. A.; Pardi, L. A.; Poussereau, S.; Sorace, L. *Chem.—Eur. J.* **2000**, *6*, 4580−4586.

(29) (a) Chandrasekhar, V.; Bag, P.; Speldrich, M.; van Leusen, J.; Kögerler, P. *Inorg. Chem.* **2013**, *52*, 5035−5044. (b) Long, J.; Habib, F.; Lin, P.-H.; Korobkov, I.; Enright, G.; Ungur, L.; Wernsdorfer, W.; Chibotaru, L. F.; Murugesu, M. *J. Am. Chem. Soc.* **2011**, *133*, 5319−5328.

(30) Cañadillas-Delgado, L.; Fabelo, O.; Pasán, J.; Delgado, F. S.; Lloret, F.; Julve, M.; Ruiz-Pérez, C. *Dalton Trans.* **2010**, *39*, 7286−7293.

(31) (a) Benelli, C.; Caneschi, A.; Gatteschi, D.; Pardi, L.; Rey, P.; Shum, D. P.; Carlin, R. L. *Inorg. Chem.* **1989**, *28*, 272−275. (b) Benelli, C.; Caneschi, A.; Gatteschi, D.; Pardi, L.; Rey, P. *Inorg. Chem.* **1989**, *28*, 275−280. (c) Benelli, C.; Caneschi, A.; Gatteschi, D.; Pardi, L.; Rey, P. *Inorg. Chem.* **1990**, *29*, 4223−4228. (d) Benelli, C.; Caneschi, A.; Gatteschi, D.; Pardi, L. *Inorg. Chem.* **1992**, *31*, 741−746. (e) Benelli, C.; Caneschi, A.; Gatteschi, D.; Sessoli, R. *Inorg. Chem.* **1993**, *32*, 4797−4801. (f) Benelli, C.; Gatteschi, D.; Sessoli, S.; Rettori, A.; Pini, M. G.; Bartolomé, F.; Bartolomé, J. *J. Magn. Magn. Mater.* **1995**, *140*−*144*, 1649−1650.

(32) Venugopal, A.; Tuna, F.; Spaniol, T. P.; Ungur, L.; Chibotaru, L. F.; Okuda, J.; Layfield, R. A. *Chem. Commun.* **2013**, *49*, 901−903.

(33) Orbach, R. *Proc. R. Soc. London, Ser. A* **1961**, *264*, 458−484.

(34) Gatteschi, D.; Sessoli, R. *Angew. Chem., Int. Ed.* **2003**, *42*, 268−297.

(35) del Barco, E.; Kent, A. D.; Hill, S.; North, J. M.; Dalal, N. S.; Rumberger, E. M.; Hendrickson, D. N.; Chakov, N.; Christou, G. *J. Low Temp. Phys.* **2005**, *140*, 119.

(36) For illustration, ac frequency scans were collected at 2.8 K and fields ranging from 2700 to 3750 Oe (spanning the sharpest magnetization drop in the hysteresis at this temperature). These scans reveal ac peaks between 3 and 5 Hz and corresponding relaxation times with very minimal field dependence (see Supporting Information Figure S13). The relaxation time decreases gradually upon traversing the fields where the drop in magnetization occurs, as might be expected for the occurrence of tunneling.

(37) Lukens, W. W.; Walter, M. D. *Inorg. Chem.* **2010**, *49*, 4458−4465.

(38) Sarachik, M. Magnetic Avalanches in Molecular Magnets. In *Molecular Magnets: Physics and Applications*; Bartolomé, J., Luis, F., Fernández, J. F., Eds.; Springer: New York, 2014.

dx.doi.org/10.1021/ic4030102 | *Inorg. Chem.* 2014, 53, 3099−3107